Localization in liquid phase separation: Coarsening and stable structures

Avanish Kumar,[1,*] Chaitanya Narayanam,[2,†] Rajesh Khanna,[2,‡] and Sanjay Puri[1,§]
[1]*School of Physical Sciences, Jawaharlal Nehru University, New Delhi-110067, India*
[2]*Department of Chemical Engineering, IIT Delhi, New Delhi-110016, India*

(Received 17 August 2019; published 31 December 2019)

Dynamics of pattern formation in self-organizing systems subjected to spontaneous suppression of diffusion through a recently proposed source-sink-boundary templating technique is presented based on three-dimensional numerical simulations. This template disorder is introduced to divide the system into three different subregions, i.e., a source (outer subregion) at higher potential and a sink (inner subregion) region at a lower potential with the help of a boundary which is at the highest potential. The boundary allows only one-way diffusion from source to sink so diffusion stops completely whenever the sink is filled to its capacity. This technique was shown to be able to spontaneously form stable and complex patterns in the source and the sink parts. While the technique is applicable to any self-organizing or phase-separating system whenever certain conditions are met, a physically realizable system of liquid films supported on chemically heterogeneous substrates which self-organizes through morphological phase separation is chosen to study the dynamics. Free-energy functional of this system shows an asymmetric double-well potential and the Maxwell's double tangent construction on this free energy gives rise to two distinct and finite equilibrium phases. Disorder is introduced in the form of chemical heterogeneity to divide the whole system into different subregions each consisting of two equilibrium phases, thus enabling more finite equilibrium points in the same system. The dynamics uncovers two different pathways for stable localized structures, viz., the defect and the direct pathway. Thinner films are likely to favor the defect pathway whereby the equilibrium pattern forms after coarsening, whereas thicker films will predominantly choose the direct pathway of pattern formation by phase separation. The final localized structure is same irrespective of the chosen pathway. The dynamics also shows that the patterns formed in the inner subregion part can be seen as a result of "localization" and those formed in the outer subregion are due to arrested diffusion under geometric or curvature constraints. Simple measures of localization in terms of free energy and its constituents are also presented. The identification of localization in the above systems opens up the possibility of a systematic approach to create controlled structures at nano- and submicrometer scales with desired shape and size. These structures constitute new building blocks of advanced and tailored materials.

DOI: 10.1103/PhysRevE.100.062803

I. INTRODUCTION

Natural structures are mostly stable and have definite shape and size. Formation of these structures is a complex process which depend on nature of forces present in the system and thermodynamic conditions. These structures emerge in the spatiotemporal evolution of nonequilibrium or far-from-equilibrium systems [1–6]. Pattern formation due to organization of matter is possible by various means, such as reaction, diffusion, or convection [7–13]. Among these processes, diffusion is the most common mechanism for self-organization and is present in almost all pattern-forming systems at all length scales. A classic example is the process of phase separation in homogeneous binary mixtures [14–17].

Phase separation can be spontaneous (in unstable systems) or by nucleation and growth (in metastable systems) [18–21]. However we should stress that there is not a sharp distinction between two regimes. The phase-separating domains coarsen by Ostwald ripening, in which the material evaporates from smaller domains and condenses into bigger ones [22,23].

Self-organizing phase-ordering systems such as unstable binary mixtures (e.g., a mixture of water and oil) result in emergent structures which coarsen with time. The primary mechanism of self-organization in such systems is diffusion which proceeds indefinitely. Therefore, the emergent structures in these systems are diffusion driven, which coarsen with time. Coarsening is a continuous process which proceeds through diffusion and stops only in the asymptotic time regime [24–26].

Also, the self-organizing emergent structures [27–30] in binary mixtures are spontaneous and outcome of the phase-separation process. One of the important issue here is that the shape and length scale of the emergent structures are not precisely defined, and they are not stable. These patterns are dictated by interfacial curvatures, and the dynamics proceeds to minimize the interfaces or domain boundaries. The thermodynamic equilibrium in such processes corresponds to the coexisting single domains of each phase separated by a well-defined boundary. In the intermediate stages of this process we get complex *flowing shapes* which are not stable as the system

*avanishkumar31@gmail.com
†nskc.iitd@gmail.com
‡rajkh@chemical.iitd.ac.in
§purijnu@gmail.com

is in a nonequilibrium state. Hence, it is a challenging task to get sustained structures in the process of phase separation and coarsening dynamics. To obtain a sustained structure in space and time we must localize the material, that is, we must stop the diffusion or the material flux.

Recently a technique has been proposed for creating stable complex structures at nano- and submicrometer scales in liquid films [31]. The proposed technique employed the mechanism of source-sink-boundary for the spontaneous cessation of diffusion in self-organizing systems. The boundary acts as a thermodynamic potential barrier which allows only one-way diffusion and functions as a one-way valve. In this article we show that the methodology presented is very robust and there exist different pathways of liquid film evolution leading to the same stable spatially localized structures. We outline in detail the intermediate dynamics of evolution and relaxation processes for different pathways.

This methodology in general can be used to localize the material flux in phase-ordering systems, e.g., in binary phase separation. Positional confinement of material in self-organizing systems such as in the binary mixtures has always been a challenging task in the perspective of diffusion dynamics (especially, confining the material in any particular subregion that exists independent of the dynamics of the surrounding region).

In recent studies [32,33], it has been shown that a liquid film (i.e., Newtonian liquid) on a solid substrate can spontaneously phase separate into two distinct finite equilibrium phases if the system is thermodynamically unstable and the free-energy functional of the system has a double-well structure. This process has been termed "true morphological phase separation" (true MPS). It has been observed that three distinct patterns emerge during the self-arrangement of the two equilibrium phases. For off-critical quenches either a "flat-film phase of lower thickness and a droplet phase of higher thickness" or "circular holes of lower thickness and cylindrical ridges of higher thickness" are observed. The bicontinuous morphology is observed for critical quenching, analogously to its counterpart of phase separation in binary mixtures.

It is well established that the conventional phase separation is governed by interfacial dynamics of domains and proceeds via their coarsening. In this process, any subregion or domain of the system is always in nonequilibrium as diffusion proceeds indefinitely and dynamics in one subregion affects others due to connected interfaces. In this article we discuss the mechanism which allows any subregion of the phase-separating system to disconnect itself spontaneously from other parts by suppressing the diffusion process. This subregion behaving as an isolated subsystem can stand alone, even though coarsening proceeds conventionally in other parts. Further, this localized domain emerges as a region of thermodynamic equilibrium which is devoid of any diffusion. Any structure in this subregion can sustain forever irrespective of dynamics in other parts of the system. *The proposed technique paves the way to regulate the intermediate dynamics of phase separation and thus enables a new route for creation of precisely defined stable localized structures.*

We also note explicitly that we neglect any exchange or movement of the material between the inner and outer subregions via the vapor phase. Such a process of liquid exchange will cause the stability of the liquid in the inner subregion. This exchange will continue until it equalizes the chemical potential in all parts of the whole system. In this perspective it is not possible to attain stable structures in the inner compartment. For practical applications to get the sustained, stable, and stand-alone shapes in the inner subregion, it should be ensured that exchange of liquid via vapor phase is not allowed.

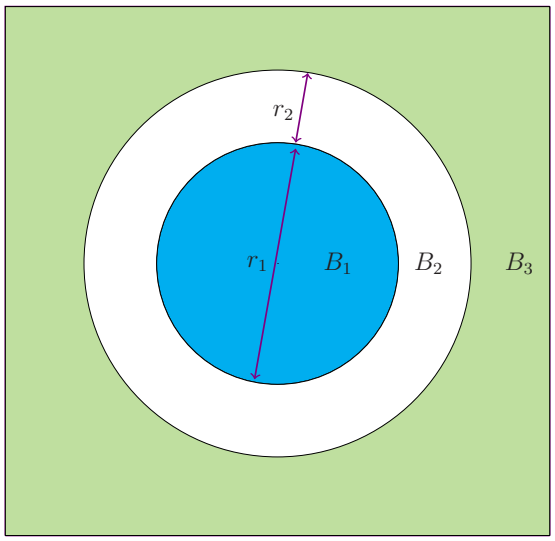

FIG. 1. Schematic diagram representing chemical heterogeneity in the system. A typical substrate with three regions (corresponding to B_1, B_2, B_3) of different wettabilities. Each region is physically and chemically homogeneous in itself and the corresponding free energy has a double-well structure with two finite minima as shown in Fig. 2. Each region arbitrarily can take any shape.

Before we outline the mechanism, we establish the fact that to create any stable structure in a subregion of a large system, two conditions must be satisfied. First, there should be flow of mass (i.e., material-flux) into the subregion until the structure is formed. Second, the flux must be stopped spontaneously to sustain the structure. These conditions suggest that there must be a gradient for material-flux with preferential directionality in the system. To achieve this we introduce disorder (in the form of chemical heterogeneity) in the thin-film system by coating the substrate with materials of different wettabilities (denoted as B) as shown in Fig. 1. Our purpose is to hold the liquid droplet in the subregion of width r_1. Note that the region r_1 can assume any random shape or any specified geometry.

In Fig. 1, the solid substrate has been divided into three subregions which correspond to three different values of B. The inner subregion of width r_1 has wettability B_1, the annular subregion of width r_2 has wettability B_2, and the outer subregion has wettability B_3. The annular part defines the boundary between the inner and outer subregions. We ensure (as verified in Sec. III) that the substrate can provide a diffusion gradient with preferential directionality if and only if it is divided into three regions with conditions as mentioned below.

Although there can be many possible combinations of B_1, B_2, and B_3, the only combination that leads to sustained and stable droplet or structure in subregion r_1 is the one with the wettabilities in order of $|B_2| < |B_3| < |B_1|$. Note that

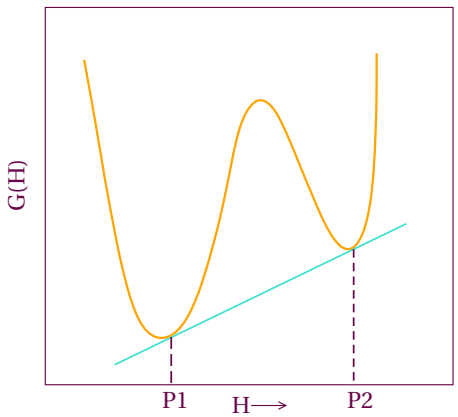

FIG. 2. Schematic diagram representing the free energy of a liquid film system resting on a substrate as shown in Fig. 1. The equilibrium phases are defined by the Maxwell's double tangent construction. Corresponding to three different regions of heterogeneity there are three double-well potentials having six minima in total as shown in Fig. 3.

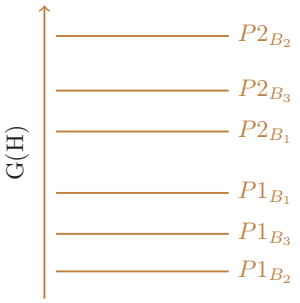

FIG. 3. Schematic diagram showing the relative order of the free energies (in arbitrary units) corresponding to the equilibrium phases in different subregions for the system as shown in Fig. 2. Note that free energy corresponding to the second equilibrium phase of the boundary is at the highest.

"true MPS" corresponds to a substrate coated with a single material which is physically and chemically homogeneous everywhere (i.e., a single value of wettability B). If $r_2 = 0$ and $r_1 \to \infty$ (i.e., r_1 fills the whole space), then we will get the homogeneous substrate coated with B_1. The same is true when $r_1 = 0$ and $r_2 \to \infty$, where we will get a homogeneous substrate with wettability B_2. If both $r_1 = 0$ and $r_2 = 0$, then again we will have homogeneous substrate with wettability B_3. Another interesting case is when one of r_1 (or r_2) is zero and the substrate has only two subregions (which we do not discuss here).

Each subregion in Fig. 1 corresponds to an asymmetric double-well free energy, schematically shown in Fig. 2. The subregions are physically and chemically homogeneous individually and facilitate two finite equilibrium phases which are obtained by Maxwells double tangent construction on the free energy (see Fig. 2). Hence each subregion can independently support true MPS. In contrast, when combined together the collective behavior and thermodynamic equilibrium of the whole system is completely different compared to the dynamics of the system with only a single wettable region.

As will be discussed in Sec. II, in the expression of the free energy $G(H)$ and its first derivative $\partial G/\partial H$ (i.e., chemical potential) and the second derivative $\partial^2 G/\partial H^2$ (i.e., spinodal parameter), the wettability B is an important parameter which takes a constant value. It can be observed from these expressions that higher the value of $|B|$ for any subregion, lower is its chemical potential (see Fig. 4). We mention explicitly that the wettabilities of sink, source, and the boundary are independent of the liquid composition, i.e., the liquid's molecular composition does not change the chemical composition of the substrate and coatings. For practical applications, it has to be ensured that the liquid composition does not modify the surface properties and the vice versa. The change in the composition of substrate due to liquid will change the wettabilities, surface energies, and hence the liquid dynamics. In the numerical simulations we have considered water as the liquid film. Also the approximation is for the Newtonian liquid.

In Fig. 1, the annular subregion (i.e., the boundary) is at the highest chemical potential and the inner region is at the lowest. Because of its design or construction, this system facilitates a directed gradient for material flux to the inner subregion. Since the boundary is at very high chemical potential, it pushes the liquid to flow in either directions, i.e., toward the inner and the outer regions. The direction of diffusion (material-flux) is preferentially toward the inner subregion due to larger differences in chemical potential. In the inner patch, coarsening will proceed until liquid attains the equilibrium height $P_{2_{B_1}}$ and completely fills the width r_1 (with circular shape shown in Fig. 1). In Sec. III we will verify this methodology for the case when the inner subregion has been given a square shape.

Once the inner subregion is filled to its capacity, i.e., it takes the shape and size of the inner patch corresponding to equilibrium thickness, diffusion stops spontaneously into this subregion and it disconnects from the other parts. There is no more material-flux to or from the inner subregion even though the gradient for diffusion exist in all over the system. Here boundary (i.e., annular subregion) works as a one-way thermodynamic valve which allows diffusion into inner subregion until the equilibrium conditions of inner patch are achieved.

Note that coarsening is fundamental to the growth of domains in any phase-separation process. The positional confinement of liquid in any subregion, and its coarsening until the achievement of equilibrium shape and size of the subregion, is an example of localized coarsening. The localized droplet can be considered a complete thermodynamically stable system in itself with well-defined domain walls. The dynamics in the outer region proceeds with coarsening, and there is self-organization of material in space and time, giving rise to simple or complex structures depending on the geometrical constraints.

Thus phase separation can result in a stable localized structure in any subregion of the system instead of flowing shapes in that subregion. We will also show that this mechanism will result in the emergence of complex structures in outer region which are stabilized by arresting of diffusion. Clearly, the localized structures are coarsening-based ripened structures. Therefore, the present methodology is completely

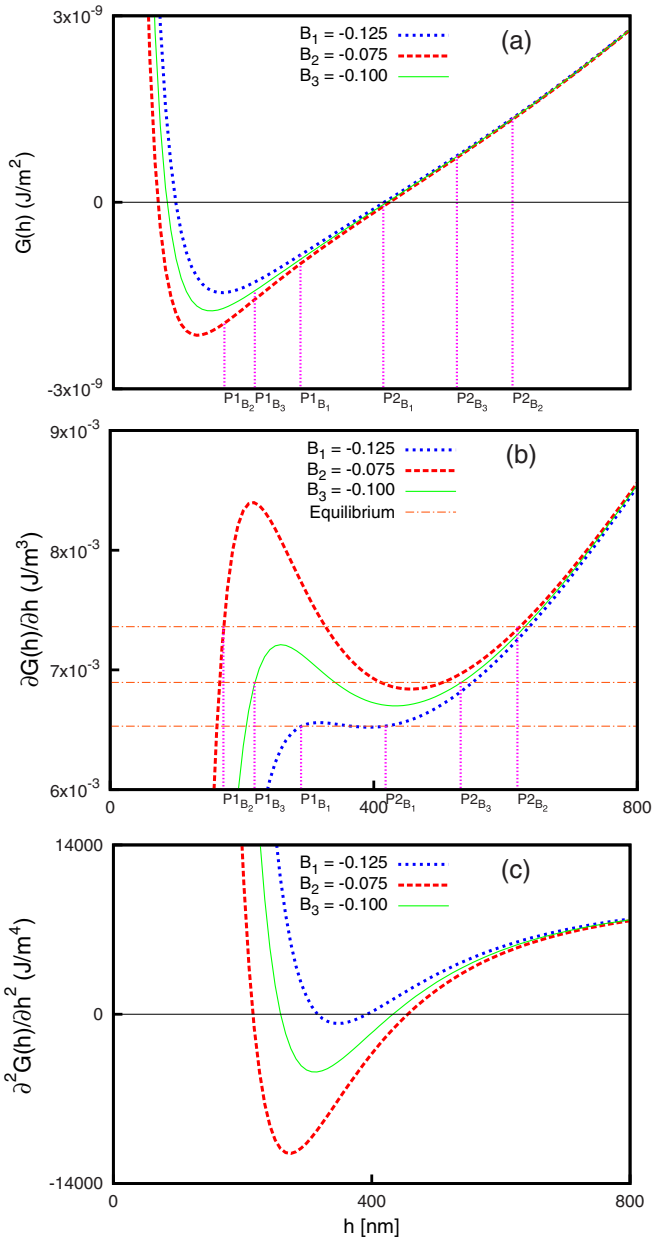

FIG. 4. Plots of (a) individual free energies, (b) chemical potentials, and (c) spinodal parameters with mean film thickness h for the three subregions (or compartments) of varying wettabilities B_1, B_2, and B_3 for the liquid-film system considered in the text.

different from the conventional templating techniques such as lithography, surface deposition, or optical masking used to create nanostructures.

This article is organized as follows. In Sec. II, we describe the mathematical model for the spontaneous "true MPS" process on chemically heterogeneous substrates. In Sec. III, we present a detailed description of the process of creating sustained and localized structures in simple liquids. Note that the use of the word *simple liquid* denotes in general the Newtonian liquid; however, our results are valid for non-Newtonian liquids such as polymers, gels, highly viscous fluids, suspensions and emulsions, blood, etc.

We outline the different mechanisms by which a system can evolve leading to the same final equilibrium structure in the inner subregion. We also describe the formation of secondary structures in the outer subregion due to the arresting of liquid by geometrical frustration and curvature constraints. We present qualitative measures such as free energy and entropy to show the microscopic behavior of liquid motion and its localization. Finally, in Sec. IV we conclude the paper with a brief summary of our work and discuss its potential applications.

II. MATHEMATICAL MODEL

To outline the equation of motion for a thin liquid film, we consider a three-dimensional (3D) (i.e., $2D+1$) Newtonian liquid film on a solid substrate in the XY plane. The thin-film evolution equation is obtained by application of lubrication approximation to the hydrodynamic equations of motion in the long-wavelength approximation limit [34–37]. The resultant thin-film equation in dimensionless form is similar to the Cahn-Hilliard equation [14–16] as:

$$\frac{\partial}{\partial t}H(X,Y,t) = \vec{\nabla}\cdot\left[M\vec{\nabla}\left(\frac{\partial G}{\partial H}\right)\right], \tag{1}$$

where $H(X,Y,t)$ is the height of the film at the point (X,Y) on a 2D substrate and time t. Mobility M in the above equation is height dependent and is given by $M(H) = H^3$. The dimensionless free-energy functional is given by

$$G(H) = \int dXdY\left[f(H) + \frac{1}{2}(\vec{\nabla}H)^2\right], \tag{2}$$

where the square gradient term represents the fluid-fluid interfacial tension and $f(H)$ is the bulk free energy, also called the excess free energy.

The excess free-energy for the liquid film surface supported on a coated substrate in the presence of a bounding fluid is given by the free-energy functional

$$f(H) = -\frac{A_c}{12\pi H^2} - \frac{A_s - A_c}{12\pi(H+D)^2} + \rho g h_0^4\frac{H^2}{2}, \tag{3}$$

where $H = h/h_0$ is the nondimensional film thickness and $D = \delta/h_0$ is the nondimensional coating thickness. Here δ is the coating thickness on the solid substrate, ρ is the density of the liquid, g is acceleration due to gravity, h is the height of the liquid film in nanometer above the coating at time t, and h_0 is the film thickness at initial time $t = 0$. The effective Hamaker constants are positive for partially wettable surfaces (A_s) and negative for completely wettable surfaces (A_c).

The dimensionless form of the excess free energy can also be written as [32,33]:

$$f(H) = -\frac{1}{6}\left[\frac{1-B_i}{(H+D)^2} + \frac{B_i}{H^2} - QH^2\right]. \tag{4}$$

In Eq. (4), $D = \delta/h_0$ is the dimensionless thickness of coating, $B_i = A_{ci}/A_s$ ($i = 1, 2, 3$ corresponding to the three subregions of the system) is a spatial variable that is always negative and $Q = 2\pi\rho g h_0^4/|A_s|$ is the force corresponding to gravity.

The corresponding thin-film equation is now given by

$$\frac{\partial H}{\partial t} = \vec{\nabla}\cdot[H^3\vec{\nabla}(f'(H) - \nabla^2 H)]. \tag{5}$$

Substitution of Eq. (4) in Eq. (5) leads to the following nondimensional form of the nonlinear equation for temporal evolution of the thin liquid film system under gravity:

$$\frac{\partial H}{\partial t} = \vec{\nabla} \cdot \left(H^3 \vec{\nabla} \left\{ \frac{1}{3} \left[\frac{1 - B_i}{(H + D)^3} + \frac{B_i}{H^3} + QH \right] - \nabla^2 H \right\} \right). \tag{6}$$

The controlled disorder is incorporated by templated nanocoating on the substrate and thus making the system under study a heterogeneous system. The value of B_i varies spatially and for regions 1, 2, and 3, it takes the values of B_1, B_2, and B_3, respectively. The linear stability analysis of Eq. (6) shows that the wavelength corresponding to the most unstable modes in each subregion B_i is

$$(L_M)_i = \frac{4\pi}{\sqrt{-f''(1)}} = 4\pi \left[\frac{1 + |B_i|}{(1 + D)^4} - |B_i| - \frac{Q}{3} \right]^{-1/2}. \tag{7}$$

The evolution of these instabilities leads to the formation of two true equilibrium phases as given by the Maxwell's double tangent construction. Note that for each of the three subregion corresponding to three different wettabilites, there are three different and distinct unstable modes $(L_M)_1$, $(L_M)_2$, $(L_M)_3$.

It is clear from Fig. 4 for the spinodal parameter that the unstable or the spinodal region corresponding to B_1 is also contained within the spinodal regions corresponding to both the B_2 and B_3. Thus the region of common instability is the spinodal region of B_1. For all the other spinodal regions, apart from that of B_1, the system may not facilitate spontaneous phase separation. Therefore, all the fluctuations leading to the spontaneous phase separation are given to the spinodal region of B_1. Also, the dominant long-wavelength fluctuations correspond to $(L_M)_1$ of the inner subregion B_1.

We mention explicitly that intrinsically there is no asymmetry for the flow in the Cahn-Hilliard equation. It is the property of substrate or surfaces and hence the surface energies (i.e., the combination of low- and high-energy surfaces) which create the different force fields in different regimes facilitating the asymmetricity in the flow. The equation of motion (i.e., the Cahn-Hilliard equation) involves the parameters dependent on the substrate properties; therefore, any surface modification will lead to a change in the flow dynamics. Experiments related to movement of liquid on low- and high-energy surfaces [38–41] at the nanoscale have been performed which clearly show the role of different energy surfaces in controlling the spreading of the liquid. The results in this paper, have been obtained by solving Eq. (6) in a $2+1$-dimensional system. Periodic boundary conditions are applied in the x and y directions and the initial condition is a uniform film surface of thickness $H = 1$ perturbed by fluctuations of amplitude $\simeq 0.01$. The system sizes were chosen in multiples of dominant wavelength, i.e., $(nL_M)^2$ (n ranging from 16 to 32). Central differencing in space with half-node interpolation was used for discretization, and Gear's algorithm, which is highly efficient for solving stiff equations, was employed for time marching.

III. RESULTS AND DISCUSSION

Figure 5 presents a typical phase diagram for a liquid film which shows the spinodal and metastable regions correspond-

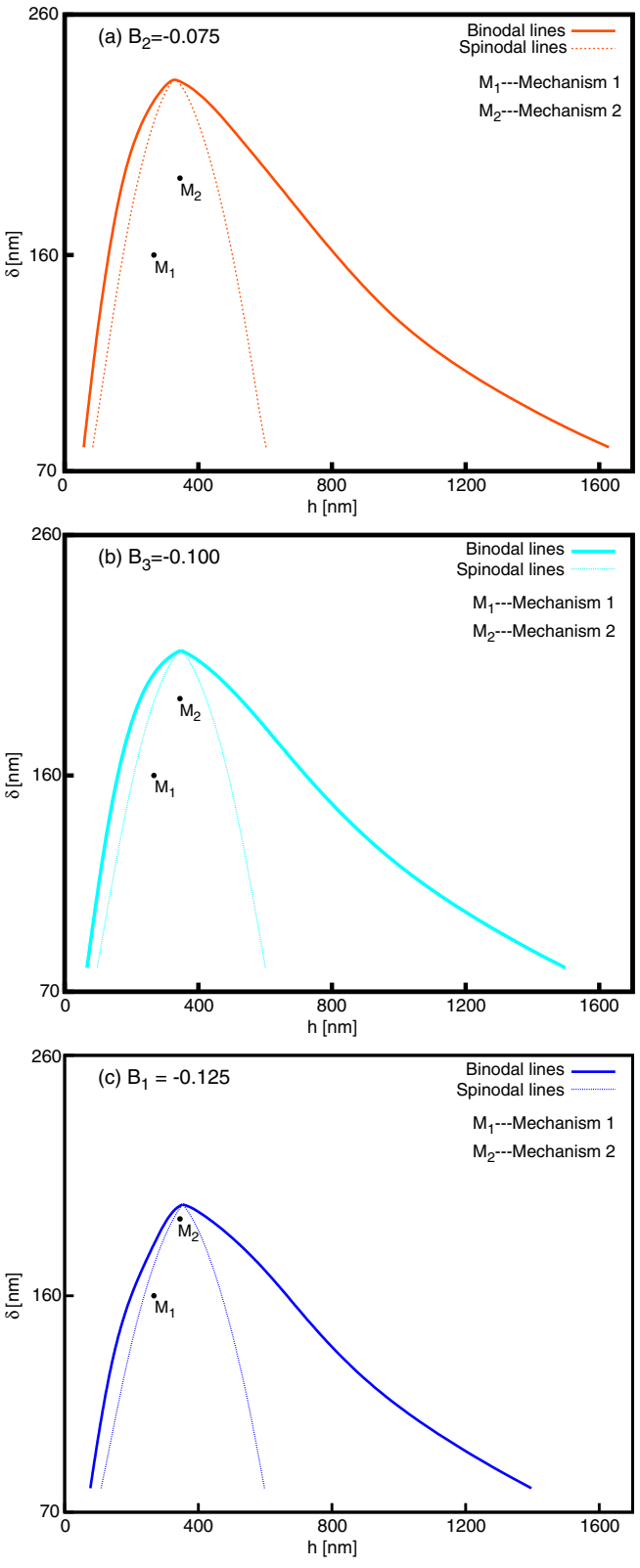

FIG. 5. The individual phase diagrams for (a) boundary, (b) outer subregion, and (c) inner subregion for the liquid film system considered in our study. The points M_1 and M_2 fall into the common spinodal region of all the three subregions corresponding to Fig. 4. M_1 corresponds to defect pathway, whereas M_2 corresponds to direct pathway. Note that δ is the coating thickness and h is the mean film thickness.

ing to the three subregions of wettabilities B_1, B_2, and B_3, respectively. The spinodal region is the region of instability where any surface fluctuation in the liquid film is amplified, spontaneously leading to morphological evolution of the film. Note that the phase diagram in Fig. 5 is a combination of three separate phase diagrams, one for each of the subregions and hence includes three spinodal and three metastable regions corresponding to each subregion. For clarity, the respective phase diagrams have been put on top of each other.

Spontaneous phase separation is possible in the system only when the initial film thickness lies in the region of common instability (i.e., the spinodal region which is common to all the subregions). From Fig. 4 it is clear that the spinodal region of B_1 is common to spinodal regions of all the three subregions. Because of asymmetricity in the free energy of the liquid film system, the phase diagram is also asymmetric.

It was observed [32,33] that true MPS proceeds through two distinct pathways depending on the initial thickness of the film. The *defect pathway* is observed for films whose initial thickness lies closer to one of the equilibrium phases and farther from the other. Hence, there is a delay between the appearances of the first and second equilibrium phases, as the second phase appears only after significant coarsening of the nonequilibrium domains (defects). Two different patterns, namely "flat-film and cylindrical droplets" and "circular holes and cylindrical ridges" are observed for defect pathway depending on whether the initial thickness is closer to the thinner equilibrium phase or thicker equilibrium phase, respectively. This pathways is analogous to off-critical quenching in the binary phase separation.

The *direct pathway* is observed for films whose thickness lies in a narrow band centered around halfway to both the equilibrium phases [33]. Both the equilibrium phases appear simultaneously for the films undergoing true MPS through a direct pathway and result in a "bi-continuous pattern" formation. The three subregions have their individual spinodals and binodals. Hence, the pathway of true MPS may vary for each of the subregions. However, in our simulation results we deal with initial film thicknesses which always lie in the common instability region. This pathways is analogous to the critical quenching in the binary phase separation.

We discuss the underlying mechanisms in the formation of stable structures by choosing a square-shaped inner subregion for illustration. Two different thicknesses corresponding to different positions (M_1 and M_2) in the unstable region of the phase are chosen to explain the evolution mechanisms of the stable structures. Figures 6 and 9 show the localization of the liquid waves for 266-nm film on 160-nm coating and 320-nm film on 192-nm coating, respectively. Random fluctuations to any unstable thin liquid film placed on a substrate amplify under the influence of intermolecular forces.

For a heterogeneous system with disorder, the instability propagates in the form of sinusoidal waves that rearrange to the likeness of the template, say, spherical rings for circular templates. The liquid races to form six equilibrium phases, two in each region, and thereafter the evolution of the film is different for the three regions. The droplets formed within the boundary are the initial ones to disappear due to the pressure gradient being highest at the boundary. The liquid in the boundary will always be at equilibrium thickness $P1_{B_2}$ and

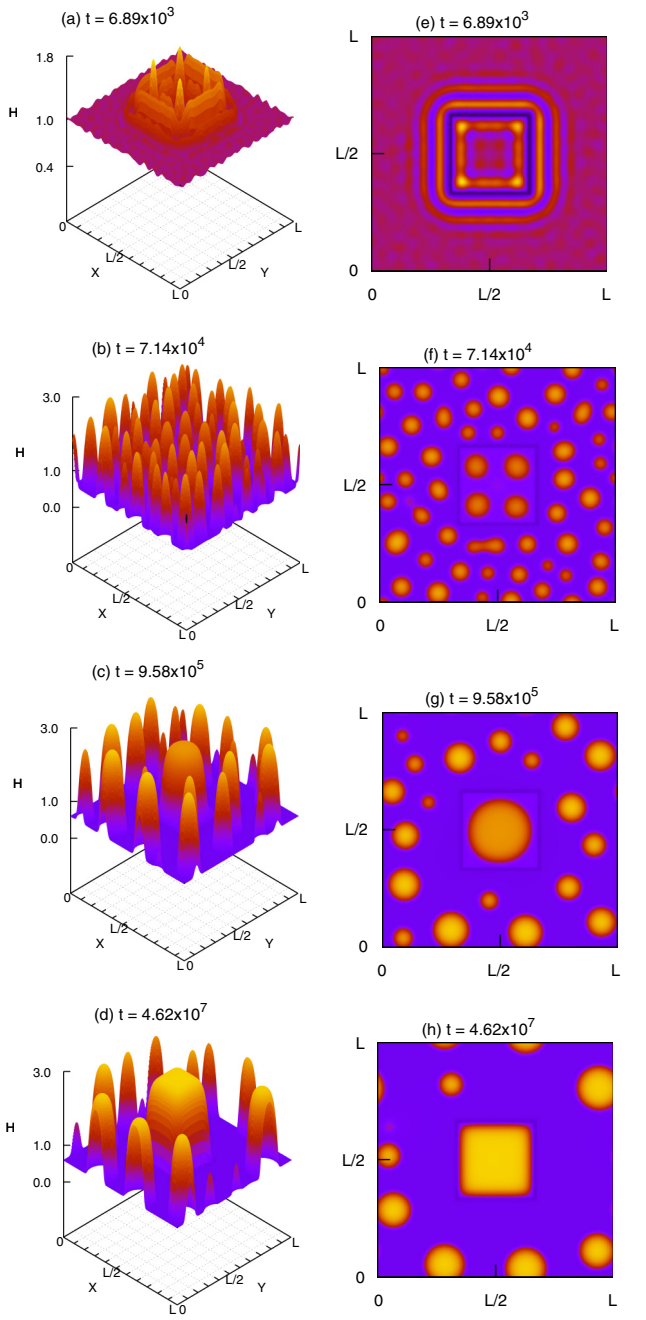

FIG. 6. Morphological evolution of a liquid film on a substrate with a square-shaped inner subregion. Panels (a)–(d) present the lateral view and panels (e)–(h) present the top view of the snapshots in the morphological phase-separation process at nondimensional time t following mechanism 1. H is nondimensional film thickness. System size is $(16L_m)^2$ and the simulation parameters are $B_{\text{out}} = -0.1$, $B_{\text{in}} = -0.125$, $B_{\text{boundary}} = -0.075$, $D = 0.6$, and $Q = 0.031$.

correspond to the flat-film phase. The direction of diffusion is always into the inner subregion until it is filled to its capacity. Hence, the structure in the inner subregion will always correspond to the equilibrium thickness $P2_{B_1}$. After the diffusion into inner subregion ceases, the leftover liquid in the outer region rearranges itself to achieve the thermodynamic equilibrium. The outer region will always have two coexisting

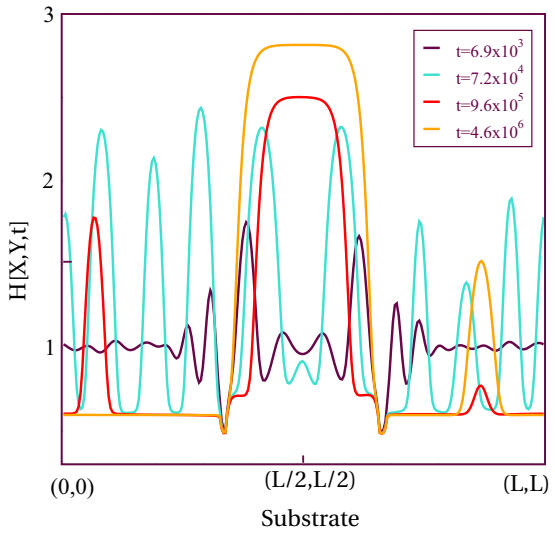

FIG. 7. Diagonal height fluctuations corresponding to the evolution morphology in Fig. 6 for the defect pathway.

phases, $P1_{B_3}$ and $P2_{B_3}$, and depending on the pathway can result in either one of the three sets of patterns explained above. However, we will observe that structures which appear in the outer subregion are constrained by geometrical constraints and thermodynamically not preferable.

The initial film thickness will not affect the final shape or size of the structure in the inner subregion but decides the mechanism of its formation. Two distinct mechanisms have been observed for the formation of localized structure depending on the position of film thickness in the phase diagram.

A. Mechanism 1

The left and right panels of Fig. 6 present the lateral and top views of the morphological evolution of a thin film on a substrate with a square-shaped inner subregion for a 266-nm film on a 160-nm coating (point M_1 in the phase diagram). The initial film thickness is closer to the thinner equilibrium phase binodal than the thicker phase. Thus, the second phase $P2_{B_1}$ will appear only after a significant amount of coarsening of the droplets. The initial fluctuations reorganize themselves into a flat film and droplets within the inner subregion. Coarsening among the droplets within the inner subregion leads to the formation of a single bigger droplet. This is the region of highest wettability and hence the direction of flow of material is always into the inner region. Thus, coarsening of this single droplet continues until it both (i) reaches the thickness corresponding to $P2_{B_1}$ and (ii) fills the entire region of the inner part. The diffusion of liquid into the subregion ceases once both the conditions are satisfied and then the structure remains localized irrespective of the dynamics in the outer region.

Figure 7 shows the diagonal heights corresponding to the evolution presented in Fig. 6 at different times. The two lowest points resembling a dip in the height correspond to the boundary (i.e., the periphery) of the inner subregion. We observe that all the bigger fluctuations in the initial stages take

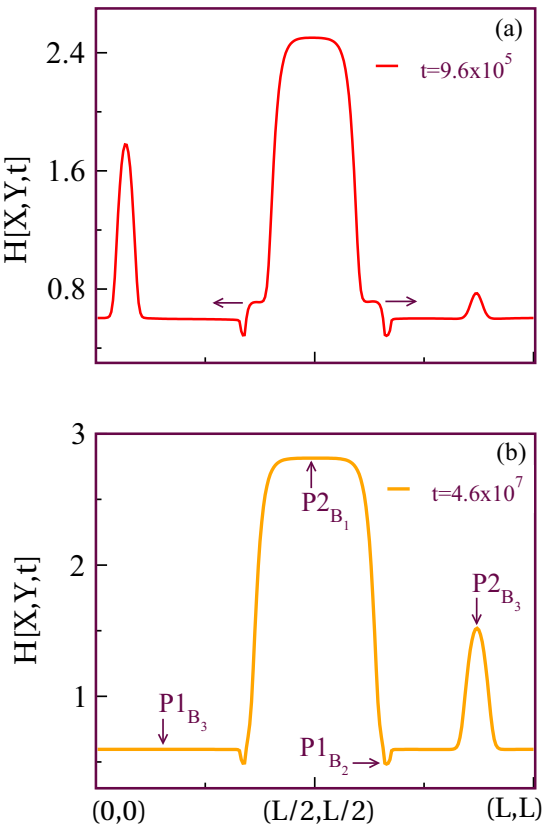

FIG. 8. Diagonal heights showing the cylindrical droplet (a) and its conversion into the square structure (b).

place at the boundary (periphery of inner subregion) points. These fluctuations grow in height with time and move laterally toward the center of the inner subregion to form a cylindrical droplet [as shown in Fig. 8(a)].

Note that the two bumps created in the droplet formation correspond to the lower thickness $P1_{B_1}$ of the inner subregion. At this stage, we have five phases in the system, i.e., two phases of the inner region, two phase of outer subregion, and one flat film phase corresponding to the annular boundary. Once the droplet is formed, it grows both in width and height to fill the squared subregion and to achieve the equilibrium structure. In this process, the bumps (i.e., the lower thickness $P1_{B_1}$) go away, giving thereby smooth interfaces at the boundary of this inner subregion. In the end, we have only four phases left in the system.

Figure 8(b) corresponds to the late stage when the inner subregion has achieved its equilibrium. The structure is ripened and is settled down. On the other hand, the outer subregion is still undergoing a nonequilibrium process and diffusion continues. The droplet in the outer region (which is marked by arrow head with $P2_{B_3}$) will grow to achieve equilibrium thickness $P2_{B_3}$ if liquid from other smaller droplets diffuses into it, or this droplet might diffuse into another droplet if the later is bigger. Note that the growth of this nonequilibrium droplet depends on the availability of the liquid.

Since $P2_{B_3}$ is higher than $P2_{B_1}$ (see Fig. 3), if there is enough liquid or material, then we will get a droplet which

is bigger in height compared to the height $P2_{B_1}$ of the square-shaped inner subregion in the asymptotic timescale.

Thus we have a system where one subregion achieves equilibrium early while the other subregion remains in nonequilibrium. The diffusion in the outer subregion stops only when the leftover material has diffused to make a bigger droplet and nothing has been left for further diffusion. If there are any geometrical constraints in the outer subregion, then the liquid movement is not free and it is restricted to move locally. Liquid diffusion is arrested thereby restricting liquid into locally stable states.

The first mechanism is more generic and proceeds according to conventional coarsening dynamics, while the second mechanism is a little unconventional.

B. Mechanism 2

Figure 9 presents the lateral view (panels on the left) and the top view (panels on the right) of the morphological evolution of a 320-nm film on a 192-nm coating (point M_2 in the phase diagram). This composition corresponds to the critical composition or mixture of true MPS [33]. The crest of the fluctuations always appears at the edge of the inner subregion and thus amplification of the initial fluctuations results in a donut or concentric-shaped structure.

The edges of this concentric structure correspond to the crests, and the hole of the structure correspond to the troughs. The initial film thickness in this pathway lies almost halfway to the binodals of both the equilibrium phases. In this mechanism, the liquid does not support formation of the thinner flat-film phase (i.e., $P1_{B_1}$) of the inner subregion. That is, only the upper thickness or the second equilibrium phase is achieved and grows vertically in the process.

Since we have chosen a critical composition, a bicontinuous structure would have formed if $r_2 = 0$ and $r_1 \to \infty$ (see Fig. 1) in this system, analogously to the spinodal phase separation in binary mixtures for critical quenches [33]. However, in this case, since the inner subregion is always at the lowest chemical potential and the liquid flow is always in this subregion, it is thermodynamically preferable to form a liquid structure of thickness $P2_{B_1}$. Therefore, the self-arrangement proceeds with the liquid filling the hole in the concentric structure. The structure as a whole then grows in height to reach $P2_{B_1}$ if it has not been achieved up to that time.

Figure 10 shows the diagonal heights corresponding to mechanism 2. *In this pathway, fluctuations which take place at the boundary (or periphery) of the inner subregion grow only vertically by filling liquid into the inner subregion. Fluctuations do not move in or out and there is no intermediate droplet formation.* The shape of the subregion is achieved by coarsening and ripening leading to stable structures with smooth interfaces. Although it appears at a first glance that sharp interfaces are formed in the morphological structures. However, the sharp edges or sharp interfaces in the liquid-gas interface is generally not observed in the perspective where the Newtonian liquid cannot sustain the shear stress or the strain. Therefore, it is hard to observe the sharp interfaces in simple liquids. Any shape taken by the liquid is basically its density profile [42].

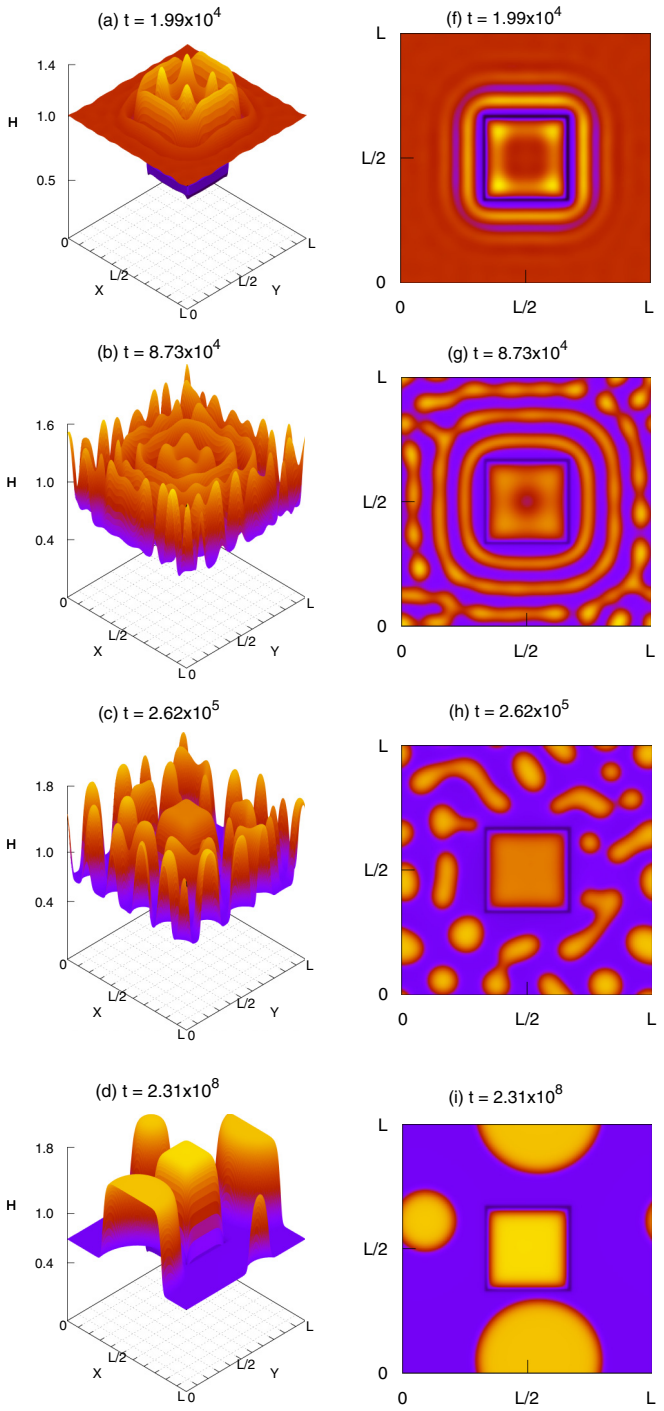

FIG. 9. Morphological evolution of a liquid film on a substrate with a square-shaped template. Left panels [(a)–(d)] present the lateral view and right panels [(f)–(i)] present the top view of the snapshots in the morphological phase-separation process at nondimensional time t following mechanism 2. H is nondimensional film thickness. System size is $(16L_m)^2$ and the simulation parameters are $B_{\text{out}} = -0.1$, $B_{\text{in}} = -0.125$, $B_{\text{boundary}} = -0.075$, $D = 0.6$, and $Q = 0.012$.

Note that in this pathway, the lower thickness $P1_{B_1}$ of the inner subregion is never formed. The final equilibrium structure is the same as in the defect pathway with only four

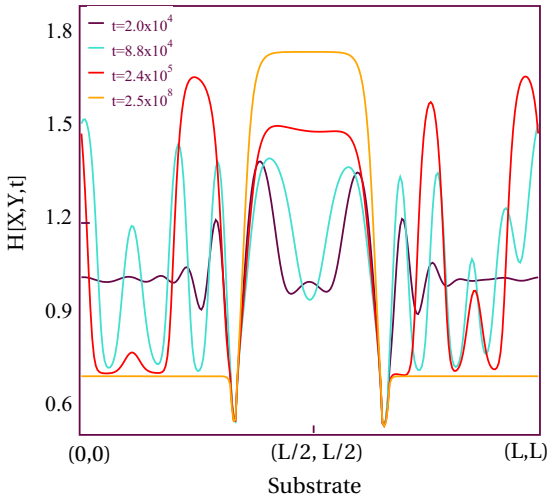

FIG. 10. Diagonal height fluctuations corresponding to evolution morphology in Fig. 9. In this mechanism the lower thickness $P_{1_{B_1}}$ of the inner subregion is never formed.

phases in which some are in equilibrium and some are in nonequilibrium.

To distinguish both the mechanisms, we need to have a better understanding of the free energy of the system. The end goal of true MPS is the minimization of total free energy, which is the sum of excess free energy and the interfacial free energy. Any self-organization has to always lead to the minimization of at least one of these if not both. For mechanism 1, as $P1_{B_1}$ appears in very early stage before $P2_{B_1}$ and the defects have to grow in size to reach $P2_{B_1}$, the defects in the inner subregion reorganize themselves into the interfacially preferable circular droplet structures, which have a higher probability to reach $P2_{B_1}$ faster. They subsequently reach $P2_{B_1}$, thus minimizing the free energy in the inner subregion and further coarsen laterally to take structures corresponding to the template of the inner subregion to minimize the free energy for the whole system.

On the other hand, for mechanism 2, amplifications in both the crests and the troughs of instability takes them equally closer to their corresponding equilibrium phases and the excess free energy is moving closer to its minimum possible value. After the appearance of the concentric structure, any rearrangement into the droplets would unnecessarily increase the interface and also disturb the dynamics of the concentric edges and the concentric hole. Any reorganization of the concentric structure would result in increasing the total free energy which is not at all preferable. Thus, the preferential route is to minimize the total free energy by filling the hole of the donut (or concentric shape) to bring it to the level of the rest of the structure.

Thus, the two different mechanisms, differ in their approach to fulfill the two guidelines of a stable structure. These mechanisms depend on the competition between height and width, i.e., which of the two will achieve their equilibrium behavior first. *In mechanism 1, the structure reaches height $P2_{B_1}$ first and then proceeds to fill the width of the inner subregion. In mechanism 2, the structure fills the inner subregion first and then proceeds to reach $P2_{B_1}$.*

These evolution figures provide a better insight into the statement that the equilibrium shape of the inner structure is independent of the pathways of evolution and the dynamics of outer subregion. It can be observed that no matter the film thickness, the liquid within the inner subregion always assumes the shape of the patch (square in this case). The length scale of the inner structure (or the domain) is the length of the inner patch. If enough liquid is available, then the liquid always fills the inner subregion first. The diffusion to and from the inner region ceases once the required conditions for the equilibrium are fulfilled.

Note that the role of boundary is instantaneous and continuous, but this role is clearly visible when the sink is filled to its capacity and more liquid cannot flow to the sink. Since the sink is at the lowest potential the gradient of flow is always toward the sink from the source but not the reverse. Also, the boundary being at the highest potential it presses the liquid with its maximum force to flow it away from the boundary toward the either side, i.e., toward source and sink. Once the sink is filled to its capacity, the boundary does not allow the liquid to flow from sink to source since the reverse diffusion is suppressed by the boundary due to its repelling nature. Therefore the flow is always unidirectional and hence the boundary fulfills the role of a thermodynamic valve and ensures only one-way diffusion.

The square- or triangle-shaped inner subregions lead to the formation of structures that are exact replicas of the templates. The liquid always fills the inner patch irrespective of the shape of the disordered region. This enables the formation of liquid structures with well-defined boundaries or interfaces and the structures with varied shapes.

Any complex structure formed is stable irrespective of the position of the inner patch within a system. Here we observe a completely at-equilibrium region in the midst of a nonequilibrium region. If we let the process continue, then we reach a thermodynamical state where we have four specific domains: (a) the localized drop within inner subregion, (b) the flat film covering the boundary area, (c) two coexisting phases that can be bicontinuous or flat-film and cylindrical drops or circular holes and ridges. We also note another very important fact about the effect of the formation of a liquid monolayer (i.e., a single spreading film) for the rest of liquid in the inner subregion where stable structures has to be obtained. If the wettability of the inner substrate is very high such that a single monolayer or precursor film of the liquid is formed first, then it will reduce the wettability of the substrate and hence it will change the dynamics for the rest of liquid flowing toward the inner or sink part. The dynamics will become very slow and this process may rule out any macroscopic structure in the sink [38].

We emphasize that no other combination of the wettabilities (i.e., chemical potentials) of the three subregions will give rise to stable structures in the inner compartment. For example, if we physically exchange the inner and outer subregions, or the wettabilities of inner and outer subregions are exchanged, then the direction of diffusion is now from inner to outer subregion. All the liquid will flow away from the inner to the outer region in this case. There will be no other structure in the inner region apart from a flat film of liquid similar to the boundary.

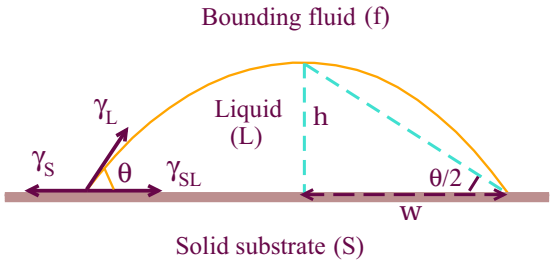

FIG. 11. Schematic diagram showing the liquid drop on a solid substrate and the Young's condition for drop equilibrium on the substrate. h is the difference between the equilibrium heights of the film. γ represents the interfacial tension and θ is the equilibrium angle between substrate and liquid.

The formation of a stable complex structure, i.e., complete inhibition of the diffusion is possible only when the size of the inner subregion is greater than a critical value such that it can hold the liquid at its equilibrium thickness. From Fig. 11, we have

$$\tan\frac{\theta}{2} = \frac{h}{w} = \frac{P2_{B_1} - P1_{B_2}}{w} \tag{8}$$

or

$$w = \left(\frac{P2_{B_1} - P1_{B_2}}{\tan\frac{\theta}{2}}\right). \tag{9}$$

Therefore the total width of the inner subregion must be greater than $2w$. Note that the height h is difference between the equilibrium thicknesses $P2_{B_1}$ and $P1_{B_2}$. It is clear from Figs. 7 and 8 for the diagonal heights that the heights $P2_{B_1}$ and $P1_{B_2}$ are the two bounds for any structure in the inner subregion.

Also, the width of the boundary should be large enough to discourage the convection of the liquid, but there is no constraint on the size of the annular boundary as long as the chemical potential of the boundary is higher than both the inner and outer subregions. However, from our numerical simulations we have observed that the difference $|B_{\text{in,out}} - B_{\text{boundary}}| > 10^{-3}$. Here B_{in}, B_{out} correspond to the wettabilities of the inner and outer subregions, respectively, and B_{boundary} is the wettability of annular boundary.

Convection of liquid is also observed in some cases where smaller domains closer to the inner subregion are pulled into the site by bulk transport.

The process of localized structure formation and the corresponding mechanisms are similar for either a single inner subregion or multiple subregions as shown in (Fig. 15). As long as the outer region has enough liquid to diffuse into the inner subregions, the process can continue without any hindrance. The structures in these subregions do not communicate with each other even if the outer surface runs out of liquid or if the wettabilities of the inner subregions vary. The suppression of diffusion happens regardless of whether the inner subregions have well-defined geometries or are completely random. Ordered or well-defined subregions have huge implications in manufacturing of microstructures of desired shape and size.

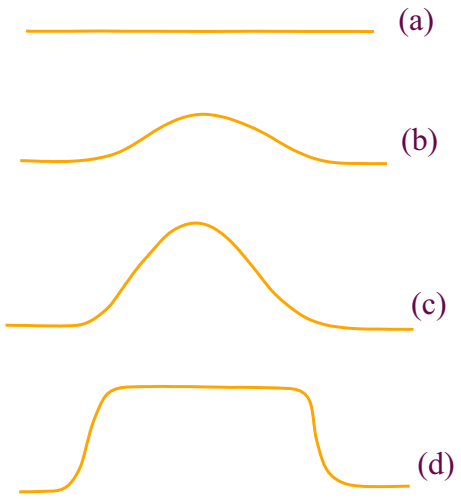

FIG. 12. Schematic diagram showing free evolution of a liquid film on a substrate under the force field described in Eq. (4). The film is initially flat and is given a small perturbation. There are no geometrical constraints in the evolution, i.e., liquid moves freely. Panels (a), (b), (c), and (d) correspond to the different stages of the evolution starting from a flat film. Note that the presence of second finite equilibrium phase (which is due to gravity in this case) determines the upper bound of the film and tries to flatten the droplet. The equilibrium behavior of film, in the absence of geometric or curvature constraints, is cylindrical droplet with flat surface as in (d).

C. Secondary structures

The combination of the inner subregion, the annular subregion, and the outer subregion constitute a *unit*. If there is only a single unit, i.e., only a single inner subregion and one annular boundary, then the outer subregion does not face any geometrical constraints in the flow of material. In the outer subregion for these cases, coarsening proceeds conventionally. Diffusion proceeds freely as shown in Fig. 12 and there is no arresting of diffusion or the material flux.

If there are more such units (i.e., multiple inner subregions and annular boundaries) in the system, then the flow of liquid in the outer subregion finds many constraints, which are due to the boundaries corresponding to annular subregion of wettabilities (B_{boundary}). The structures then formed in the outer subregion are not conventional and may take any random or complex geometry. The shape and size of these structures are governed by three parameters, namely (a) leftover liquid in the outer subregion, (b) available space in the outer subregion, and (c) geometrical constraints (or the curvature) of the boundary.

For bigger inner subregions, most of the material or liquid is employed to achieve the equilibrium structure and, hence, smaller amounts of liquid are available in the outer subregion. The arrangement of this leftover liquid now depends on the available space in the outer subregion. In this case, if the available space in the outer subregion is more with no constraints in liquid flow, then it again follows the free evolution and the resulting patterns are same as shown if Fig. 12.

If a large space is enclosed within the boundaries, such that the width of the space is much greater than $2a$, where $2a$ is the minimum width required to hold a liquid droplet of height $h = P2_{B_3} - P1_{B_3}$, then a cylindrical droplet is formed

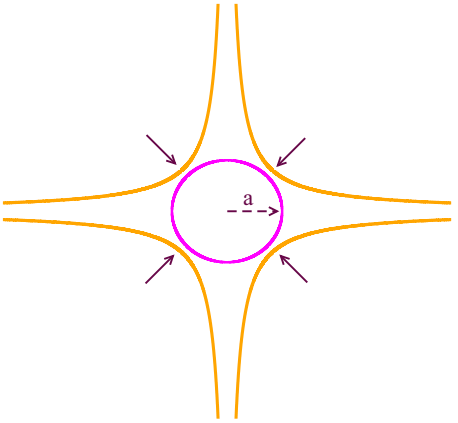

FIG. 13. Schematic diagram showing the arresting of liquid and structures obtained in outer subregions under the geometrical constraints. Bent curves represent boundaries enclosing some part of the outer subregion. Arrowheads represent the region of high pressure gradient. Depending on the amount of enclosed volume liquid can take its natural shape (i.e., droplet) or any frustrated shape (see Fig. 14) dictated by the curvature of the boundaries. A liquid droplet is formed if the enclosed volume or space is much greater than the volume corresponding to the width 2a, where 2a is the minimum width to hold a liquid droplet.

as shown in Fig. 13. $P2_{B_3}$ and $P1_{B_3}$ are the equilibrium thicknesses corresponding to the outer subregion. Also, $a = (P2_{B_3} - P1_{B_3})/(\tan\theta/2)$ and the minimum liquid volume is $\pi a^2 h$.

If the enclosed volume is less than $2a$, then on the availability of liquid, the structure starts mimicking the curvature of the boundaries (Fig. 14). As the pressure gradient

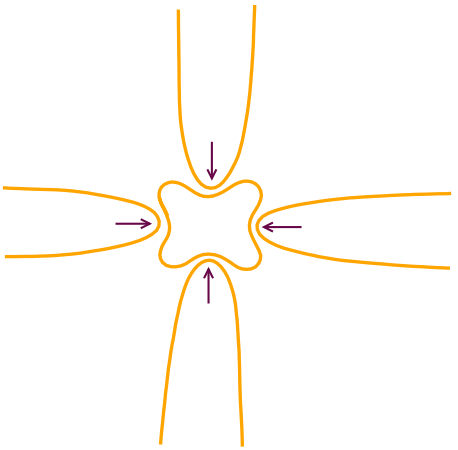

FIG. 14. Schematic diagram showing a frustrated shape in the outer subregion formed under the curvature constraints. The enclosed volume is not sufficient for the free evolution of liquid, it is more constrained. Liquid is not free to take its natural shape; it is arrested and under these constraints it tries to attain the best possible shape. Note that the state taken by the liquid is not the lowest free-energy state and does not correspond to thermodynamical equilibrium. From our numerical simulations we conclude that geometrical constraints sometimes govern the thermodynamics. Depending on the nature of the curvature the shape taken by liquid varies accordingly.

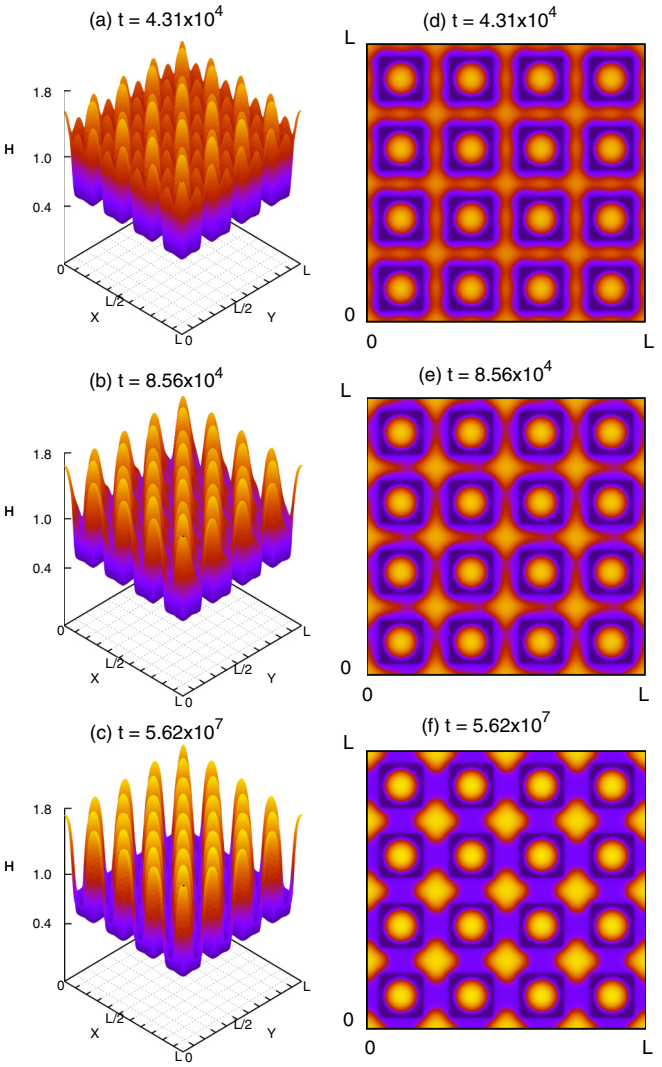

FIG. 15. Evolution of secondary structures unrelated to the template. Left panels [(a)–(c)] present the lateral view, and the right panels [(d)–(f)] present the corresponding top view of the snapshots in the morphological phase-separation process at nondimensional time t. H is nondimensional film thickness. System size is $(16L_m)^2$ and the simulation parameters are $B_{\text{out}} = -0.1$, $B_{\text{in}} = -0.125$, $B_{\text{boundary}} = -0.075$, $D = 0.6$, and $Q = 0.031$.

is very high at the boundaries, liquid or material tries to flow toward the lower pressure gradient regions. Since the motion of the liquid is constrained, it is not able to evolve freely. It gets frustrated and arrested between enclosed spaces. Figure 15 shows the formation of secondary structures with the variation of leftover volume and leftover liquid in the outer subregion.

The spontaneous cessation of diffusion in the inner subregion, formation of smooth and well-defined interfaces, multiple units (or multiple inner subregions), the intelligent movement of liquid in the surroundings (outer subregions), and their arresting leading to the secondary structures are all the building blocks for technology to manufacture complex structures. Figure 16 show some variation of enclosed space and leftover liquid leading to different secondary structures.

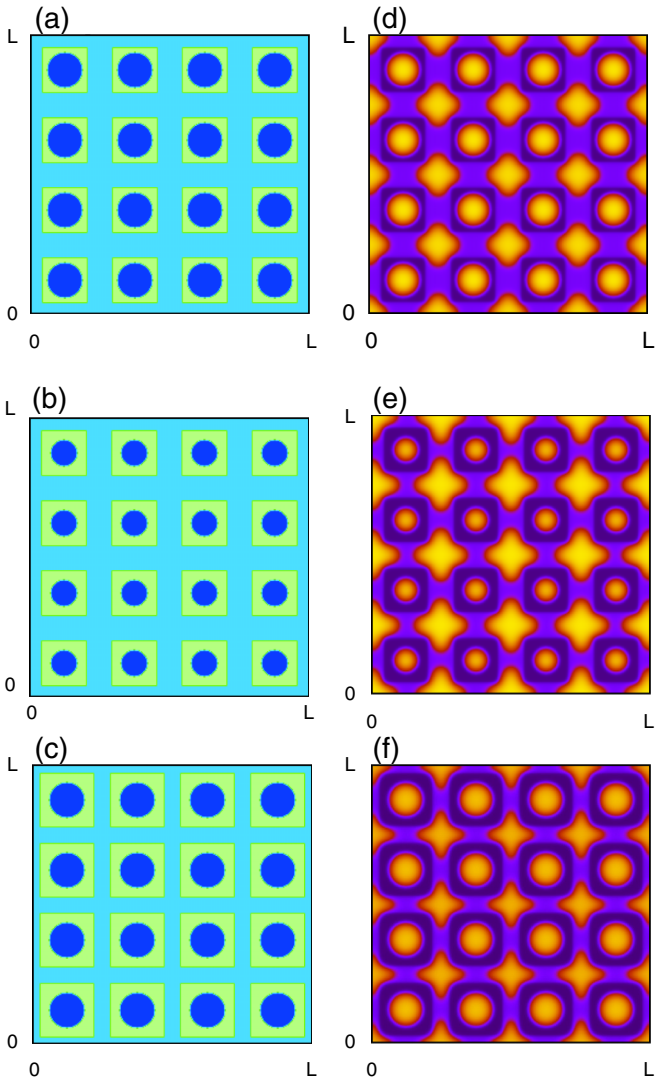

FIG. 16. Contour plots for the systems with arrested secondary structures and localized primary structures (right panels) in the two-dimensional (xy) plane. Left panels [(a)–(c)] correspond to the template, and right panels [(d)–(f)] denote the corresponding numerical simulation results. System size is $(16L_m)^2$ and the simulation parameters are $B_{\rm out} = -0.1$, $B_{\rm in} = -0.125$, $B_{\rm boundary} = -0.075$, $D = 0.6$, and $Q = 0.031$.

Figure 17 presents a few possible 3D complex structures that can be obtained by 2D templates. These structures can both be sharp or curved and can support many variations both within and outside the low potential subregion and, most importantly, they are stable.

The technique presented in this paper can be implemented to create nature-inspired stable complex structures [43,44]. In many recent studies it is shown that the liquid phase separation inside the cell cytoplasm is an important mechanism to regulate the intracellular mechanisms [45,46]. Different organelles in the cytoplasm undergo phase separation to organize and form liquid droplets. These liquid droplets coarsen and make macromolecular organisms [47–54]. Their stability and sustainability is very important for new emergent phenomena. We believe that our study can be helpful to understand and to model such systems.

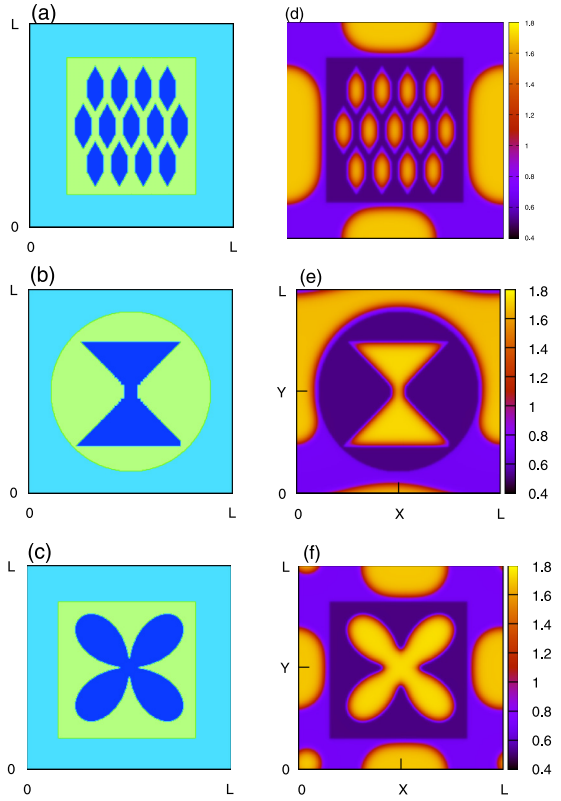

FIG. 17. Formation of stable complex 3D structures [(d)–(f)] on 2D templates [(a)–(c)]. H is nondimensional film thickness. System size is $(16L_m)^2$ and the simulation parameters are $B_{\rm out} = -0.1$, $B_{\rm in} = -0.125$, $B_{\rm boundary} = -0.075$, $D = 0.6$, and $Q = 0.031$.

D. Microscopic measures of localization

From our discussions it follows that the material is localized in the square inner subregion (Figs. 6 and 9). To confirm the validity of this claim we give some measures which characterize the microscopic behavior of the phase-ordering system and the system's dynamics. We have also observed from the formation of secondary structures that material is arrested during the coarsening.

We note here the clear distinction between "arresting" and "localization." In the arrested state, i.e., for secondary structures, any further perturbation, or removal of any constraint in the outer subregion, may allow the liquid to diffuse and rearrange again. This can result into new secondary structures. On the other hand, external perturbation do not have any effect on the localized structures, i.e., the shape and size of the structure are always maintained or retained. *Localization is the consequence of suppression of diffusion.* In our methodology diffusion stops spontaneously after the ripening of the structure in the inner subregion has taken place. Any perturbation, and the dynamics in the other parts of the system does not affect this localized structure. We emphasize that localized structures are the ripened structures. In the following paragraphs we describe and characterize the localization process by free energy (interfacial and excess) and the entropy calculations.

Excess free energy F_e is the bulk energy and depends on the thickness profile of the film. Rearrangement of the bulk

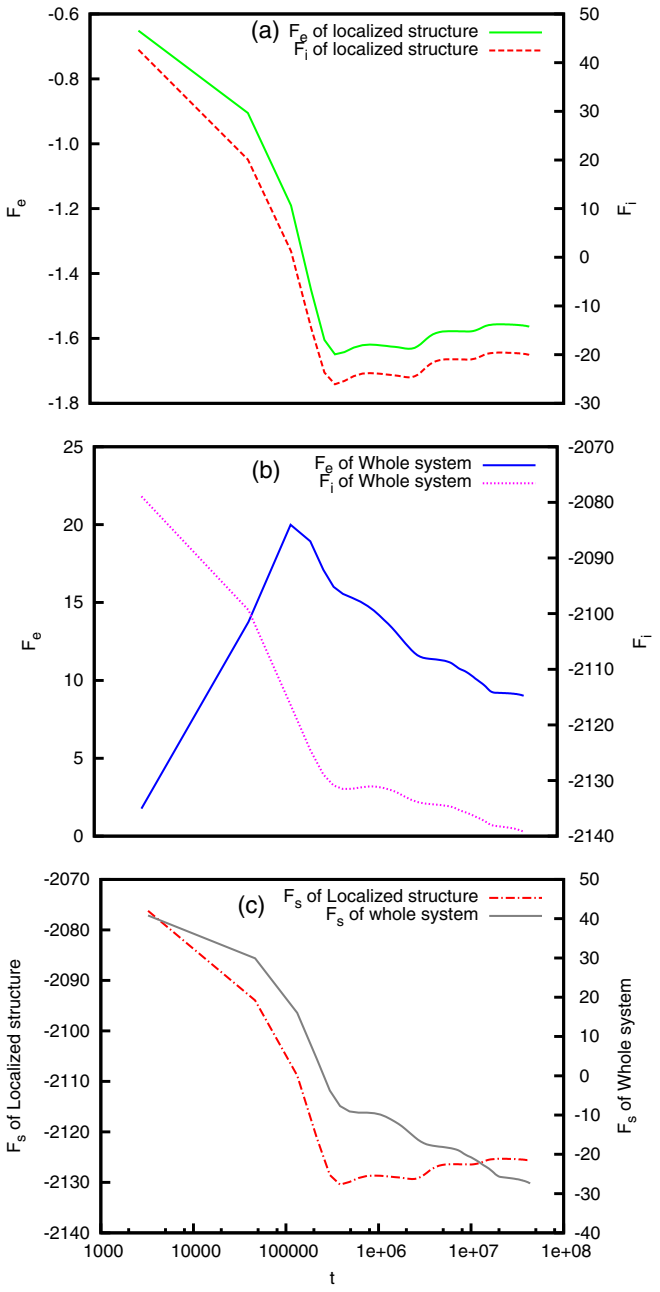

FIG. 18. Variation of excess (F_e), interfacial (F_i), and total ($F_s = F_e + F_i$) free energy with time for the system presented in Fig. 9. Panel (a) presents F_e and F_i for the localized structure. Panel (b) presents F_e and F_i for the whole system. Panel (c) presents the total free energy F_s for both the localized structure and the whole system.

(i.e., material) minimizes the excess free energy. On the other hand, interfacial energy F_i is the energy associated with the interfaces or the domain boundaries in the system. Any phase ordering system proceeds with minimization of the total free energy (F_s) which is the sum of ($F_e + F_i$). The net interfacial free energy and the excess free energy of the thin-film system in nondimensional units are given by

$$F_i = \int \frac{1}{2}(\nabla H)^2 dX dY \tag{10}$$

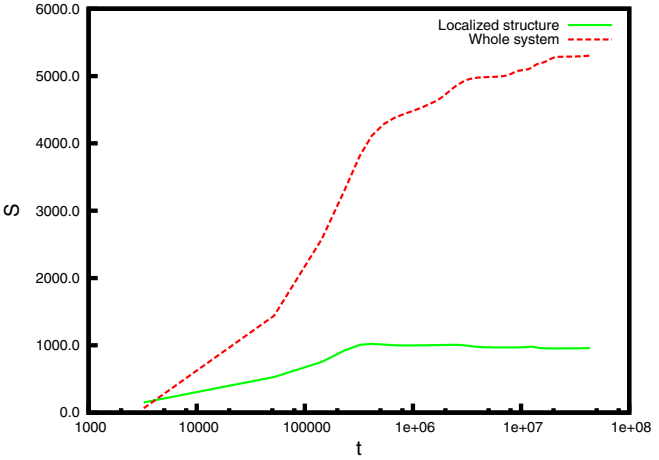

FIG. 19. Variation of entropy (S) with time (t) for the localized structure and the whole system presented in Fig. 9.

and

$$F_e = \int f(H) dX dY, \tag{11}$$

respectively.

Also, the entropy of the system is calculated to get an idea of the phase-ordering dynamics and microscopic arrangement leading to localization. At each time instant t, the entropy S in terms of height fluctuations, $H(X, Y, t)$, is

$$S = -N k_B \sum_i H_i \ln H_i, \tag{12}$$

where H_i is the height fluctuation (order parameter) at the ith grid point. Here N denotes the total number of grid points in system and k_B is the Boltzmann's constant.

Figures 18 and 19 present the variation of excess, interfacial, total free energy, and entropy of the system, respectively, with time for both the square-shaped inner subregion and the whole system presented in Fig. 9. For the inner subregion, the net excess free energy and the interfacial free energy decrease with time until the structure in inner subregion is filled (top panel of Fig. 18). The free energies assume a constant value once the structure is localized. Gradual decrease in the free energies can be observed as the structure grows to reach $P2_{B_1}$ and due to decreasing interface.

The excess and interfacial free energies for the whole system decrease with time, thus giving a thermodynamical validation to the process (middle panel). The initial increase in the excess free energy of the whole system can account for the secondary structures which are interfacially not allowed and the bulk of the system is not able to attain its natural shape. The bottom panel of Fig. 18 shows that the total free energy in the localized structure becomes constant once the system has completely achieved its shape and size, and there is no further dynamics in the inner subregion. On the other hand, there is always a decrease in total energy of the whole system since it takes a longer time for the whole system to relax into a minimum free-energy state.

The variation of entropy with time presented in Fig. 19 further validates the localization of the structure. The net

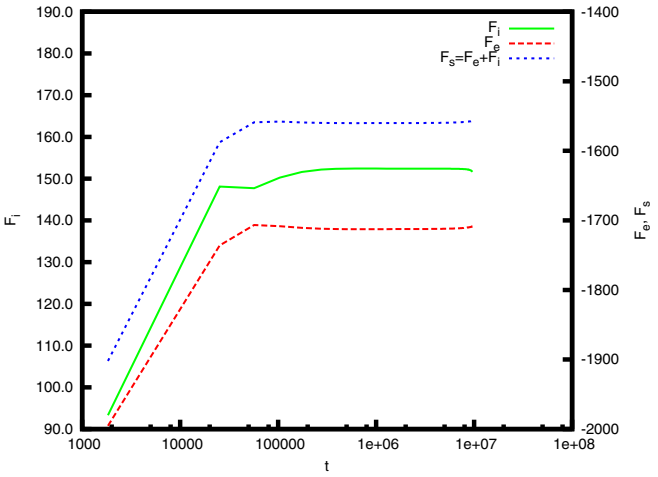

FIG. 20. Variation of excess (F_e), interfacial (F_i), and total ($F_s = F_e + F_i$) free energy with time for secondary structures only for the system presented in Fig. 15.

entropy for the localized structure becomes constant, while the entropy of the whole system increases with time.

Figure 20 presents the variation of net free energy of the system with time for the secondary structures presented in Fig. 15. It is interesting to observe that in the case of secondary structures the total energy as well as the individual contributing energy terms increase with time. This can be attributed to the geometric constraints encountered in the outer subregion as these constraints restrict the free movement of liquid. In this case, instead of minimization of interfaces we observe formation of more interfaces due to arresting of liquid in different parts of the outer region.

The excess free energy of the system also increases with time and becomes constant once all the domains in the system are at equilibrium. The interfacial free energy accurately captures the affect of geometrical constraints. The net interface increases with time since the secondary structures formed are not interfacially preferable but are forced to assume their shapes by geometrical constraints. The effect of the increased interface is clearly observable in the total free energy. Note that the secondary structures are not in the minimum free-energy states. It appears that state of secondary structures are in metastable or in locally stable state.

Note that the question of classical localization has been a subtle issue and has been observed in very few systems. It was pointed out by P. W. Anderson that localization in classical wave propagation is a phenomenon which should be easily observed in carefully prepared systems [55]. It was mentioned that although great complexity may be encountered, the classical localization can be very important to the number of highly interesting and practical systems, e.g., paints, porous media, etc. [55].

IV. SUMMARY

In summary, we have discussed the technique and different mechanisms to localize the material in any subregion of a self-organizing, phase separating large system where diffusion is the primary mechanism. The essentials of this technique is the spontaneous suppression of diffusion by using a thermodynamic potential barrier. This methodology enables to regulate the phase-separation dynamics in the intermediate stages of coarsening processes.

The present methodology shows that in a single large system we may create many subsystems each having a different dynamics and flow rate. Phase separation in fact functions as a redistribution of material into different compartments. This leads to the dynamic equilibrium in the system because different parts correspond to different equilibrium conditions irrespective of diffusion gradient. Note that if we remove the liquid from the inner subregion the diffusion again starts to complete the structure and continues until it retains its shape. This is an example of dynamical localization.

The stable localized structures are ripening based structures, i.e., the structures are formed in their natural timescale and coarsening proceeds until the full shape and size has been achieved. The thermodynamic potential barrier ensures their stability. Apart from the primary localized structures, we have shown the formation of the secondary complex structures by arrested diffusion, which in general are not in thermodynamically preferable states.

The prerequisites of the technique are (a) the free-energy functional of the liquid film system should facilitate a common tangent construction, i.e., free energy must contain two finite equilibrium phases; (b) the system should be divided into three compartments (inner, annular, and outer), each with different wettabilities (i.e., solid substrate is coated with three different materials); and (c) the inner region should be the most wettable and the annular region (i.e., boundary) should have the least wettability. This organization of three subregions constitutes a self-regulating *unit* which provides a gradient for material flux with preferential directionality. Material flows from outer compartment to the inner compartment filling to its capacity. Diffusion ceases spontaneously once the inner subregion acquires the equilibrium structure defined by free energy. Note that system may contain only one such unit or may be decomposed to contain many such units.

Depending on whether the thin film follows a "defect pathway" or the "direct pathway" of true MPS, we observe two different evolution mechanisms for localized structures in the inner compartment. The final structure is always identical to the template of the inner region irrespective of the mechanism. Also, the shape of the structure is independent of the individual strengths of the coatings, the dynamics in the outer subregion, number of self-regulating *units*, and the position of the units in the system.

We observe that the spontaneous suppression of material flux is observed only if liquid fills the inner subregion while attaining the lower equilibrium thickness of the boundary (i.e., the annular compartment) and the higher equilibrium thickness corresponding to the thicker equilibrium phase of inner subregion. The lack of diffusion into the inner compartment, and the absence of lower equilibrium thickness of the inner compartment in the final stages, leads to the formation of smooth interfaces, which in turn are the building blocks of complex structures. The higher the number of self-regulating units in a system, the higher the ability of the system to form secondary complex structures. The secondary structures in the system are regulated by the "leftover liquid"

and the "available space." Formulation of the present problem clearly shows that it is possible to have structures by both localized coarsening and arrested diffusion in the same system.

The technique explained in this article has been shown to effectively generate stable liquid structures observed in nature. The principles of technique and results presented here can be easily translated to the systems of gels and polymers also. The structures that can be created by this technique have wide range of applications in biomimetics, microfluidics, nanofabrication, nanomedicine, molecular and cell biology, and transport phenomena.

[1] M. C. Cross and H. Greenside, *Pattern Formation and Dynamics in Nonequilibrium Systems* (Cambridge University Press, Cambridge, 2009).
[2] J. P. Gollub and J. S. Langer, Rev. Mod. Phys. **71**, S396 (1999).
[3] E. Jantsch, *The Self-Organizing Universe* (Butterworth-Heinemann, Oxford, UK, 1979).
[4] P. S. Stevens, *Patterns in Nature* (Little Brown & Company, Boston, 1974).
[5] M. C. Cross and P. C. Hohenberg, Rev. Mod. Phys. **65**, 851 (1993).
[6] D. Walgraef, *Spatio-Temporal Pattern Formation* (Springer Verlag, New York, 1997).
[7] A. J. Koch and H. Meinhardt, Rev. Mod. Phys. **66**, 1481 (1994).
[8] S. Kondo and T. Miura, Science **329**, 1616 (2010).
[9] J. E. Pearson, Science **261**, 189 (1993).
[10] R. Kapral and K. Showalter (Eds.), *Chemical Waves and Patterns* (Kluwer, Netherlands, 1995).
[11] E. Meron, Phys. Rep. **218**, 1 (1992).
[12] S. Chandrasekhar, *Hydrodynamic and Hydromagnetic Stability* (Oxford University Press, Oxford, 1961).
[13] G. Ahlers, S. Grossmann, and D. Lohse, Rev. Mod. Phys. **81**, 503 (2009).
[14] J. W. Cahn and J. E. Hilliard, J. Chem. Phys. **28**, 258 (1958).
[15] J. W. Cahn, Acta Metall. **9**, 795 (1961).
[16] J. W. Cahn, J. Chem. Phys. **42**, 93 (1965).
[17] J. W. Cahn, Trans. Metall. Soc. AIME **242**, 166 (1968).
[18] V. P. Skripov and A. V. Skripov, Usp. Fiz. Nauk **128**, 193 (1979).
[19] P. G. Debenedetti, *Metastable Liquids Concepts and Principles* (Princeton University Press, Princeton, NJ, 1996).
[20] J. D. Gunton and M. Droz, *Introduction to the Theory of Metastable and Unstable States* (Springer Verlag, New York, 1983).
[21] V. P. Skripov, *Metastable Liquids* (John Wiley, New York, 1974).
[22] P. W. Voorhees, J. Stat. Phys. **38**, 231 (1985).
[23] P. W. Voorhees, Annu. Rev. Mater. Sci. **22**, 197 (1992).
[24] A. J. Bray, Adv. Phys. **43**, 357 (1994).
[25] S. Puri and V. K. Wadhawan, *Kinetics of Phase Transition* (CRC Press, Boca Raton, FL, 2009).
[26] R. C. Desai and R. Kapral, *Dynamics of Self-Organized and Self-Assembled Structures* (Cambridge University Press, Cambridge, UK, 2009).
[27] J. D. Halley and D. A. Winkler, Complexity **13**, 10 (2008).
[28] J. D. Halley and D. A. Winkler, Complexity **14**, 10 (2008).
[29] T. D. Wolf and T. Holvoet, Emergence versus self-organization: Different concepts but promising when combined, in *ESOA 2004, LNCS Vol. 3464*, edited by S. Brueckner *et al.* (Springer-Verlag, Berlin Heidelberg, 2005).
[30] B. L. Hu, J. Phys.: Conf. Ser. **361**, 012003 (2012).
[31] C. Narayanam, A. Kumar, S. Puri, and R. Khanna, J. Phys. Chem. C **123**, 13958 (2019).
[32] C. Narayanam, A. Kumar, S. Puri, and R. Khanna, Langmuir **33**, 3341 (2017).
[33] A. Kumar, C. Narayanam, R. Khanna, and S. Puri, Phys. Rev. E **96**, 062804 (2017).
[34] R. V. Craster and O. K. Matar, Rev. Mod. Phys. **81**, 1131 (2009).
[35] A. Sharma and R. Khanna, Phys. Rev. Lett. **81**, 3463 (1998).
[36] P. G. D. Gennes, Rev. Mod. Phys. **57**, 827 (1985).
[37] P. G. D. Gennes, F. Brochard-Wyart, and D. Quere, *Capillarity and Wetting Phenomena: Drops, Bubbles, Pearls, Waves* (Springer Verlag, New York, 2004).
[38] F. Heslot, A. M. Cazabat, P. Levinson, and N. Fraysse, Phys. Rev. Lett. **65**, 599 (1990).
[39] R. Mukherjee and A. Sharma, Soft Matter **11**, 8717 (2015).
[40] K. Koch and R. Grichnik, Philos. Trans. R. Soc. Lond. A **374**, 0183 (2016).
[41] J. Drelich, E. Chibowski, D. Desheng Meng, and K. Terpilowski, Soft Matter **7**, 9804 (2011).
[42] Wei-Heng Shih and D. Stroud, Phys. Rev. B **32**, 804 (1985).
[43] M. Sarikaya, C. Tamerler, A. K. Y. Jen, K. Schulten, and F. Baneyx, Nat. Mater. **2**, 577 (2003).
[44] P. W. K. Rothemund, Nature **440**, 297 (2006).
[45] R. Wedlich-Söldner and Timo Betz, Phil. Trans. R. Soc. B **373**, 0103 (2017).
[46] E. L. Elson, E. Fried, J. E. Dolbow, and G. M. Genin, Annu. Rev. Biophys. **39**, 207 (2010).
[47] Y. Shin and C. P. Brangwynne, Science **357**, eaaf4382 (2017).
[48] M. Feric, N. Vaidya, T. S. Harmon, D. M. Mitrea, L. Zhu, T. M. Richardson, R. W. Kriwacki, R. V. Pappu, and C. P. Brangwynne, Cell **165**, 1686 (2016).
[49] S. C. Weber and C. P. Brangwynne, Cell **149**, 1188 (2018).
[50] C. F. Lee, C. P. Brangwynne, J. Gharakhani, A. A. Hyman, and F. Julicher, Phys. Rev. Lett. **111**, 088101 (2013).
[51] H. Zhang, S. Elbaum-Garfinkle, E. M. Langdon, N. Taylor, P. Occhipinti, A. A. Bridges, C. P. Brangwynne, and A. S. Gladfelter, Mol. Cell **60**, 220 (2015).
[52] E. M. Langdon, Y. Qiu, A. G. Niaki, G. A. McLaughlin, C. A. Weidmann, T. M. Gerbich, J. A. Smith, J. M. Crutchley, C. M. Termini, K. M. Weeks, S. Myong, and A. S. Gladfelter, Science **360**, 922 (2018).
[53] S. Boeynaems, S. Alberti, N. L. Fawzi, T. Mittag, M. Polymenidou, F. Rousseau, J. Schymkowitz, J. Shorter, B. Wolozin, L. V. D. Bosch, P. Tompa, and M. Fuxreiter, Trends Cell Biol. **28**, 420 (2018).
[54] E. Dolgin, Nature **555**, 301 (2018).
[55] P. W. Anderson, Philos. Mag. B **52**, 505 (1985).